The performance analysis of a photo/thermal catalytic Trombe wall with energy generation

Xiaojian Duan[1], Chao Shen[1*], Dingming Liu[2] and Yupeng Wu[2]

1. School of Architecture, Harbin Institute of Technology, Key Laboratory of Cold Region Urban and Rural Human Settlement Environment Science and Technology, Ministry of Industry and Information Technology, Harbin 150090, China
2. Department of Architecture and Built Environment, Faculty of Engineering, the University of Nottingham, Nottingham NG7 2RD, U.K.

*Corresponding author: Chao Shen, chaoshen@hit.edu.cn

Abstract

The Trombe wall (T-wall) has gained significant attention as an advanced building envelope capable effectively harvest solar energy. Improving the functionality and performance of the T-wall is critical for achieving energy-saving and positive energy buildings. This study focuses on enhancing the functionality and performance of the T-wall by incorporating with photovoltaic (PV) panels and aluminum panels in the T-wall chamber. Additionally, the PV panels and aluminum panels are laminated with photocatalyst and thermal materials to optimize their energy harvesting capabilities. In this photo/thermal catalytic Trombe wall system, the air within the wall system moves upwards due to thermal pressure and sweeps over the surface of the catalytic material when exposed to solar irradiation. Through the combined effects of solar energy and catalytic oxidation, the cold and dirty air in the chamber undergoes heating and purification processes, resulting in the desired heating effect while significantly improving the overall air quality within the environment. The experimental results highlight that the novel T-wall system offers a multifunctional solution that addresses electricity generation, heating, and improvement of indoor air quality. The main findings of this study are as follows: (1) During the period from 9:00 to16:00, the T-wall system demonstrates the ability to provide a range of 6.25 kJ/mol to 17.74 kJ/mol of heat and 0.075 kWh to 0.372 kWh of electricity per day. (2) In terms of indoor air quality improvement, the T-wall system exhibits a one-way sterilization efficiency of bacterial aerosols ranging from 0.204 to 0.347. (3) The comprehensive performance of the system was found to be optimal when the system spacing is 25 cm. (4) In terms of the layout of UV light, it was observed that at the top and bottom of the system yielded better sterilization efficiency.

Keywords: T-wall; sterilization; the severe cold region; catalytic oxidation; energy production.

1. Introduction

With the rapid development of society, there has been a growing focus and concern about building energy consumption in recent years [1-3]. Currently, buildings account for a substantial 40% of total global energy consumption [4]. The energy consumption for heating, ventilation, and air conditioning (HVAC) represents more than 50% of the total energy consumption of buildings [5]. As a clean energy source, solar energy has the potential to reduce fossil energy consumption and carbon emissions in buildings. T-Wall, as an advanced building envelope that can effectively harvest solar energy, is gaining increasing attention. The T-wall utilizes solar radiation to facilitate airflow within the chamber, making use of the innovated feature not only minimize the energy needed for room heating but also enhance air circulation and improve indoor air quality [6-8]. The T-wall offers an exceptional solution for achieving remarkable ventilation performance. By utilizing solar energy to drive airflow and empower natural ventilation, it efficiently combines ventilation technology with advanced building envelope technology [9].

Several researchers have focused on optimizing the construction of the T-wall to improve its performance [10-12]. Ji et al. [13] incorporating PV cells onto the glazing cover of a conventional T-wall. The experimental findings demonstrated that this innovative approach achieved average electrical efficiency of 10–11%. Moreover, the room equipped with the novel T-wall experienced a maximum temperature increase of 14.42°C. Kong et al. [14] proposed a novel design that is double-layer phase change T-wall with multiple phase change. Though optimization, this design resulted in a significant increase in indoor temperature during winter, ranging from 0.3 to 6.6°C. Furthermore, it achieved a notable reduction in heat flux by 1.8% to 75.7%. Zhang et al. [15] proposed a novel T-wall with heat pipes, which efficiently reduce heat loss by an average of 56%, the cumulative heat loss was decreased by 5.29 kWh/m^2. Building upon this concept, Zhang et al. [16-18] further combined the thermoelectric module and a PV module with T-wall, creating a hybrid wall system. This innovated hybrid wall system offered multiple functionalities, including year-round electricity, space heating in heating seasons, and cooling in cooling climate. Zhu et al. [19] and Duan et al. [20] explored the combination of phase change materials (PCM) with the T-wall. They focused on determining the optimal phase change temperature and investigated the suitable PCM range for integration with the T-Wall. He et al. [21] introduced a Venetian solar collector wall by incorporating a louver within the air gap to selectively cover the absorbent cover. The new type of T-wall can improve room temperature and thermal environment while minimizing the space heat load to a significant extent.

To further expand the capabilities of the T-wall, researchers have begun exploring the integration of indoor air quality (IAQ) control technology with the T-wall. Given the heightened emphasis on creating a healthy living environment, particularly in light of the COVID-19 pandemic, enhancing IAQ has become an essential and unavoidable requirement [22-24]. Bioaerosols transmission, as one of the indoor air pollutants, poses a significant threat to public health, especially in enclosed indoor environments [25-27]. In the severe cold region of China, characterized by long, cold winters, people tend to avoid opening windows for ventilation to maintain room warmth. Consequently, Chinese energy efficiency standards [28,29] impose stringent requirements on building airtightness in these region. This leads to limited exchange of indoor air with the outside environment, resulting the accumulation of pollutants within the building. As a result, individuals face an high risk of infection due to the heightened concentration of pollutants in enclosed spaces [30-32]. Photocatalysis is considered as a new sterilization method in disinfection of pathogenic bacteria [33]. It not only exhibits a strong sterilization effect but also effectively decomposes the endotoxin produced by bacteria with low side effects. This characteristic demonstrates its great potential for bactericidal and antibacterial activities [34-36]. This findings have important implications for the control of respiratory infectious diseases within buildings [37]. He et al. [38] and Yu et al. [39] have conducted research on combining photocatalytic oxidation with T-wall. In their study, they utilized the UV light in solar radiation to initiate photocatalytic purification reaction. Yu et al. [40] combined the photocatalytic technology with a T-wall, enabling simultaneous space heating and indoor air purification. This system achieved impressive results, with a daily air heating efficiency of 41.3% and a total generated volume of fresh air reaching 249.2 $m^3/(m^2*day)$.

Additionally, thermal catalytic is also a commonly used sterilization method. It is often more efficient than photocatalysis due to its high energy consumption. Thermal catalytic offers several advantages, including high removal efficiency, simple equipment, and the absence of secondary pollution [41]. Under solar irradiation, the air temperature within the T-wall chamber can reach a range of 60–100°C [42]. It is important to note that a temperature of 45°C has the ability to inhibit the self-repair mechanisms of bacteria's DNA and RNA of bacteria, while the temperature above 55 °C can efficiently destroy bacterial DNA and RNA [43]. Yu et al. [44] propose a novel T-wall based on thermal sterilization. The T-wall demonstrates an average daily air thermal efficiency of 0.46, showcasing excellent energy-saving and purification performances in the heating season. A series of experiments [45] and numerical studies [46] have also been conducted to further investigate its performance.

Currently, the newly proposed T-wall faces certain challenges, including low system efficiency and incomplete functionality. It is worth noting that the reported papers primarily concentrate on thermal efficiency and inorganic purification efficiency of the novel T-wall. Only a limited number of studies have explored the potential of the novel T-wall for electricity generation, heating, and sterilization. The optimum spacing of the T-wall and the optimum position of the system's UV light strips have not been clearly determined yet. in light of these challenges, it is both meaningful and necessary to optimize the structural parameters of the T-wall and enhance its functionality. To accomplish this objective, the present study was carried out to propose an advanced envelope based on the T-wall. The novel T-wall chamber has an increased flow path and a larger contact area between the pollutants and the catalytic material, which improves the purification efficiency. Additionally, the integration of PV panels within the chamber allow for generation of electrical power. The air flowing inside the chamber due to the thermal pressure carries away the heat from the PV panels and increases the efficiency of electricity generation [47]. In this work, the main works included that: (1) a novel T-wall was proposed, and conducted the performance analysis of heating, electricity generation, and sterilization efficiency (2) the structural parameter of the novel T-wall was optimized. (3) The sterilization efficiency of the system was further enhanced by the arrangement of UV light strips in the chamber of the T-wall. The placement of the UV light strips in the chamber was investigated. With this study, a multi-functional wall that integrates building envelope with solar energy systems becomes a viable possibility. This advancement serves as a valuable reference for the implementation of energy-saving practices, the realization of positive energy buildings, and the effective control of the indoor environment. By combining various functionalities into a single system, this research contributes to the pursuit of sustainable and efficient building designs.

2. System description

Fig. 1 shows the schematic diagram of the novel T-wall. The components of the novel T-wall consist of high-transmission glass, PV panels with photocatalytic and thermal catalytic coatings, aluminum panels with thermal catalytic coatings, a chamber, thick walls, and an air inlet and air outlet. The high transmission glass and the thick walls form the T-wall chamber which is connected to the indoor environment. Air inlet and air outlet are set at the top and bottom of the thick walls to allow air to circulate between the chamber and the room.

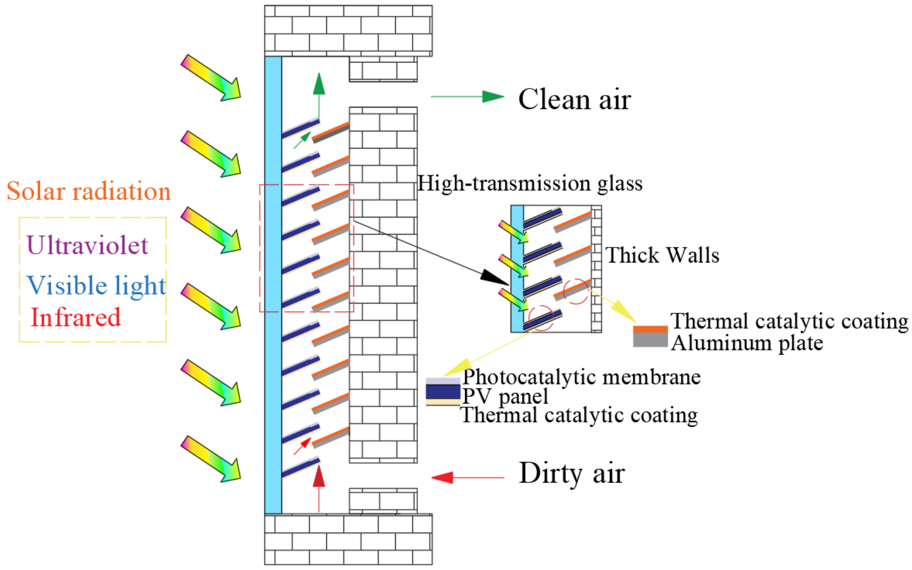

Fig. 1. The schematic diagram of the novel T-wall

In the T-wall chamber, cold air from the room enters through the lower air inlet. As the solar irradiation heats the air within the chamber, it creates thermal pressure, causing the air to flow upwards. To enhance the performance of the chamber, the PV panels have been integrated with aluminum panels in a baffle-like configuration. This design increases the distance traveled by the airflow within the chamber, allowing for a more extensive contact between the pollutants and the catalytic material.

Following the airflow and heating process, the catalytic reaction takes place within the T-wall chamber, causing the pollutants to be decomposed. As a result, the clean air leaves the chamber through the upper air outlet, establishing a circulation with the indoor air and heating the room at the same time.

When sunlight reaches the PV and aluminum panels, the ultraviolet part of the solar radiation undergoes a photocatalytic reaction on the TiO_2 membrane present on the surface of the PV panels. Simultaneously, the visible part of the solar radiation that reaches the PV panels is converted into electricity, which can be utilized to power various indoor appliances and systems or stored for later use. The remaining infrared part of the solar radiation is converted into thermal energy, which raises the temperature of the PV and aluminum panels. In addition to the aforementioned processes, the thermal catalytic material applied to the PV and aluminum panels exhibits a high a high absorption rate of solar radiation in the infrared part. Driven by the high temperature, a thermal catalytic reaction takes place when the catalytic temperature is approached. This reaction effectively degrades the airborne pollutants present in the T-Wall system. With the integration of these mechanisms, the novel T-wall design enables a comprehensive and efficient utilization of sunlight, ensuring optimal energy utilization and air purification capabilities.

3. Experiment

The experiment was conducted during the period of October to November 2022, with a duration of 9:00 - 16:00. The experiment setup was situated on the roof of a school located in Harbin, Heilongjiang Province, China. To simulate the presence of airborne pollutants, a certain concentration of Serratia marcescens suspension was prepared and uniformly sprayed into the environmental chamber using an aerosol generator. The environmental parameters of the environmental chamber have been set to simulate an indoor environment of 22°C and 60% relative humidity. The bacterial aerosol is mixed in the environmental chamber and then enters the novel T-wall under thermal pressure. The air inlet and air outlet were closed during the night time.

3.1 Photo and thermal catalytic material

In this study, a TiO_2 membrane was employed as the photocatalytic material on the surface of the PV panels. TiO_2 will produce strong oxidizing substances under ultraviolet light. Among them, $\cdot O_2^-$ and $\cdot OH$ has strong oxidation. As shown in **Eq. (1)**

to **Eq. (7)** Strong oxidizing substances will destroy the permeability of the bacterial membrane and DNA / RNA structure to achieve the effect of sterilization.

$$TiO_2 + hv \rightarrow h^+ + e^- \quad (1)$$

$$h^+ + H_2O \rightarrow \cdot OH + H^+ \quad (2)$$

$$e^- + O_2 \rightarrow \cdot {O_2}^- \quad (3)$$

$$H_2O + \cdot {O_2}^- \rightarrow HO_2 \cdot + OH^- \quad (4)$$

$$2HO_2 \cdot + e^- + H_2O \rightarrow H_2O_2 + OH^- \quad (5)$$

$$H_2O_2 + e^- \rightarrow \cdot OH + OH^- \quad (6)$$

$$H_2O_2 + O_2 \rightarrow \cdot OH + H^+ \quad (7)$$

Due to the half-wave loss of reflected light in the film, some optimization of the membrane thickness is required. As shown in **Eq. (8):**

$$D = \frac{(2k+1)\lambda_0}{4} (k = 1, 2, 3 \ldots \ldots) \quad (8)$$

D is the calculated film layer thickness, λ_0 = 550 nm. According to the theory of optical membrane layer design, when the membrane layer thickness d conforms to **Eq. (8)**, it can weaken the intensity of reflected light and increase the intensity of transmitted light, which plays a role in increasing the transmission. In this experiment, the thickness of the photocatalytic membrane is 62 μm, which satisfies the condition of the increased transmission film.

Fig. 2 shows the I-V curves for the PV panels. Without the membrane, the peak power is 0.055 w. However, with the inclusion of membrane, the peak power output decreased slightly to 0.051 w, representing approximately 92.7% the power output achieved without the membrane. Hence, it can be concluded that the addition of the photocatalytic membrane has not much effect on the power generation efficiency of the PV panel.

(a) **(b)**

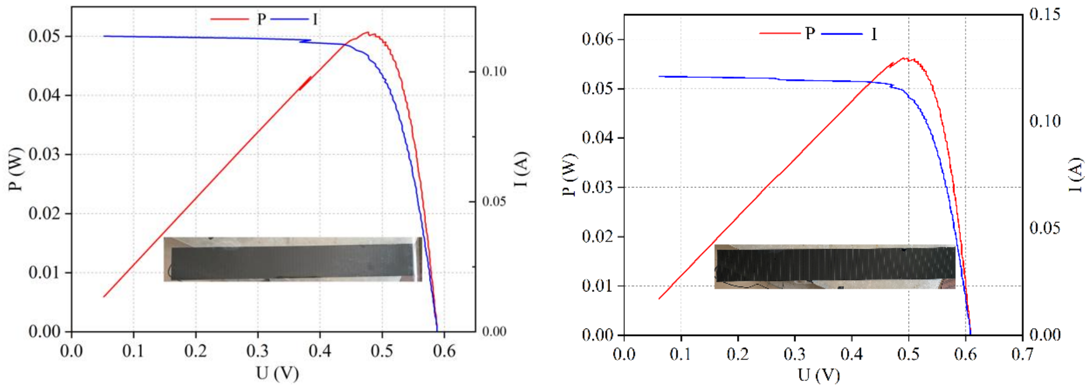

Fig. 2. Photograph of the PV panels **(a)** with film and **(b)** without film

In this experiment, MnO_x - CeO_2 was used as the thermal catalytic material. MnO_x - CeO_2 absorbs the infrared and visible wavelengths of sunlight and serves two purposes in the T-Wall system. Firstly, it helps in indoor heating by capturing solar energy. Secondly, it facilitates thermal, aiding in the degradation of pollutants. When combined with bacteria, MnO_x - CeO_2 can effectively destroy the bacterial cell membranes through infrared-triggered heat therapy, converting infrared radiation into heat and achieving photothermal conversion, using high temperatures to purify microorganisms. MnO_x - CeO_2 can also release metal particles that will pass through the cell membrane and destroy cell components after contacting bacterial cells [33,48].

However, the application of thermal catalytic is limited because its catalytic effect is unstable, and its sterilization performance is not as good as photocatalysis. Therefore, in this study, thermal catalysis was only used as a secondary means of indoor air purification and the main means of purification is photocatalysis.

3.2 Experimental set–up

In order to study the heat production, electricity production, and bacterial sterilization performance of the novel T-wall, an experimental test system was set up. **Fig. 3** shows the schematic diagram and photos of the experimental setup of the novel T-wall. Thermocouples were arranged at the air inlet and outlet of the novel T-wall to monitor temperature, and Petri dishes were arranged to sample bioaerosol concentrations. The temperature data were recorded using a paperless recorder and transferred to the computer. In the environmental chamber, electric heaters and ultrasonic humidifiers were arranged to simulate the room air parameters. The parameter values set for the environmental chamber were 22°C and 60% RH. Proportion integration differentiation (PID) is used to control the ambient parameters in the environmental chamber to maintain the set values. A hot-wire anemometer was also arranged in the middle of the T-wall to test the airflow speed inside the T-wall. The dimensions of the experimental set–up are presented in **Table 1**.

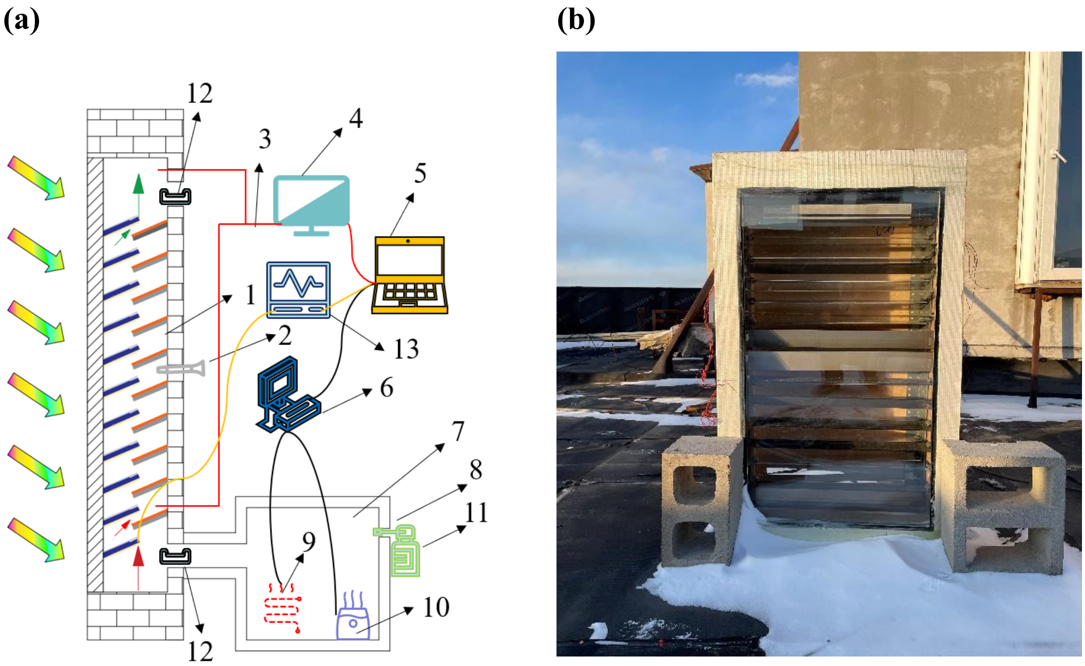

Fig. 3. The **(a)** schematic diagram and **(b)** photograph of the experimental set–up. **(1)** The novel T–wall. **(2)** Hot-wire anemometer. **(3)** Thermocouple. **(4)** Data acquisition instrument. **(5)** Computer. **(6)** Proportion integration differentiation controller. **(7)** Environmental chamber. **(8)** Pressure hole. **(9)** Electric heater. **(10)** Ultrasonic Humidifier. **(11)** Aerosol generator. **(12)** Petri dish. **(13)** IV-curve tester.

Table 1. The dimensions of the experimental set–up.

Components	Values (Length × Width ×Height)

T-wall	0.6 m × 0.3 m × 1.2 m
Environmental chamber	0.6 m × 0.6 m × 0.6 m
Pressure hole	0.02 m × 0.02 m (Ignore Width)
Air inlet or Air outlet	0.15 m × 0.6 m (Ignore Width)

The PV panels used in this study were purchased from Advanced Solar Power (Hangzhou) Inc. The specification parameters of the used PV panels under standard testing conditions (solar radiation: 1000 W/m^2, testing temperature: 25°C) are listed in **Table 2.**

Table 2. The specification parameters of per PV panel.

Parameters	Values
Model	ASP 600x80-73
Length	600 mm
Width	150 mm
Thickness	3.2 mm
Maximum Power (Pmax)	5.2 W
Voltage at Maximum Power (Vmp)	42.0 V
Current at Maximum Power (Imp)	0.123 A
Temperature coefficient of maximum power	−0.214%/°C

Experimental test parameters include temperature, airflow velocity, electrical parameters, solar radiation intensity, and bacterial aerosol concentration. Electrical parameters were recorded every 1 minute using the IV-curve, to which the PV panels were connected. A hot-wire anemometer measured the wind speed in the middle of the chamber. Thermocouples recorded the inlet and outlet air temperatures of the novel T-wall. The thermocouple was connected to the data collector, and the data was recorded every 10 seconds. The experimental accuracies of the measuring instruments are shown in **Table 3.**

Table 3. The accuracies of the main experimental measuring apparatus.

Apparatus	Model	Measuring parameter	Accuracy
Hot-wire anemometer	KANOMAX	Airflow velocity	± 0.01 m/s
IV-curve	PROVA – 200A	Electricity generation	1% of V ± 0.09V, 1% of I ± 9 mA
Thermocouple	TT–T-30	Temperature	± 0.5°C

In this experiment, Serratia marcescens was used as the bioaerosol. The safety level of Serratia marcescens is BSL-1(biological safety level of 1). This kind of bacterium can produce red dendritic colonies after 24-36 h incubation at 20-35°C, which is not harmful to the individuals involved in the experiment, and its particle size and density are representative. The method of bioaerosol sampling has been mentioned in the previous study, using Luria-Bertani agar for bioaerosol sampling.

The heat production and power generation potential of the novel T-wall was investigated in the severe cold region of China (**Section 4.1**), the structural parameters of the new T-wall were optimized, and the optimal spacing between chambers was analyzed (**Section 4.2**). The degradation efficiency of different concentrations of Serratia marcescens, at different moments, was also tested (**Section 4.3**). Finally, the effect of the layout of the UV light strips based on the self-generated power of the new T-wall was analyzed (**Section 4.4**).

4. Results and discussions

4.1 The performance of heating, electricity generation, and sterilization efficiency

The meteorological data in Harbin was tested. **Fig. 4.** shows the tested solar radiation intensity on sunny and cloudy days in Harbin, spanning from October 27th to November 20th. The subsequent investigation and comparison for the T-wall systems were conducted based on the performance calculations on sunny and cloudy days. The average solar radiation intensity of sunny and cloudy days is 527.6 W/m^2 and 272.2 W/m^2, respectively. The indoor temperature and relative humidity were set at 22°C and 60%, respectively. During the experiment, the indoor upper and lower ventilation baffles were kept in an open status from 9:00 to 16:00. To maintain the desired indoor conditions, electric heaters or ultrasonic humidifiers were activated when the air temperature and relative humidity in the airflow channel fell below the setting air temperature and relative humidity.

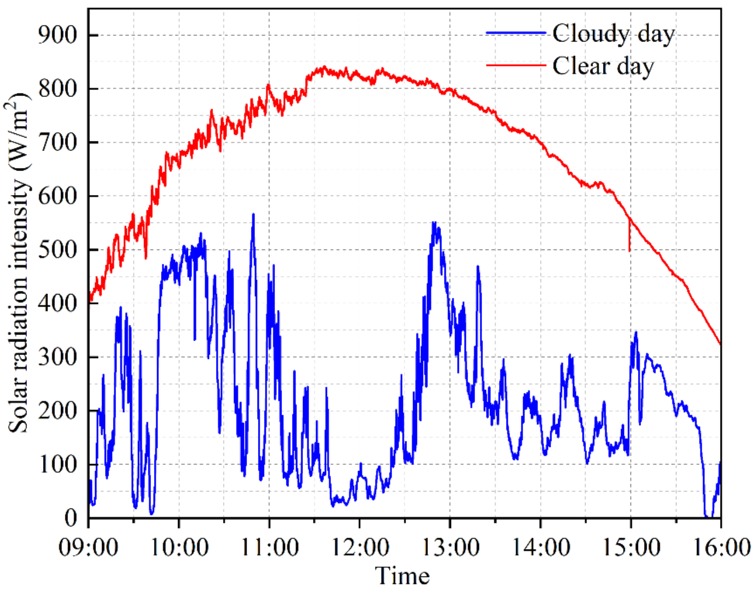

Fig. 4. The tested solar radiation intensity on sunny and cloudy days in Harbin

Fig. 5. shows the electricity generation per PV panel on cloudy and sunny days. During

the test period, the average power of the T-wall system is 3.41 W on sunny days and 0.62 W on cloudy days. The average power presents a similar variation trend with the solar radiation intensity. On sunny days, the power generated by the T-wall system approached its maximum of 4.14 W at 12:15 p.m. However, on cloudy days, the power generation did not exhibit a clear pattern or regulation. The cumulative power generation for a full day was recorded as 0.0248 kWh on sunny days and 0.005 kWh on cloud days. Considering that the T-wall system consists of 12 identically arranged PV panels, the cumulative power generation for a full day can range from 0.06 kWh to 0.298 kWh. It can be seen that meteorological data has a great effect on the power generation of the novel T-wall system. The power generation on sunny days is approximately 4.96 times higher compared to that on cloudy days.

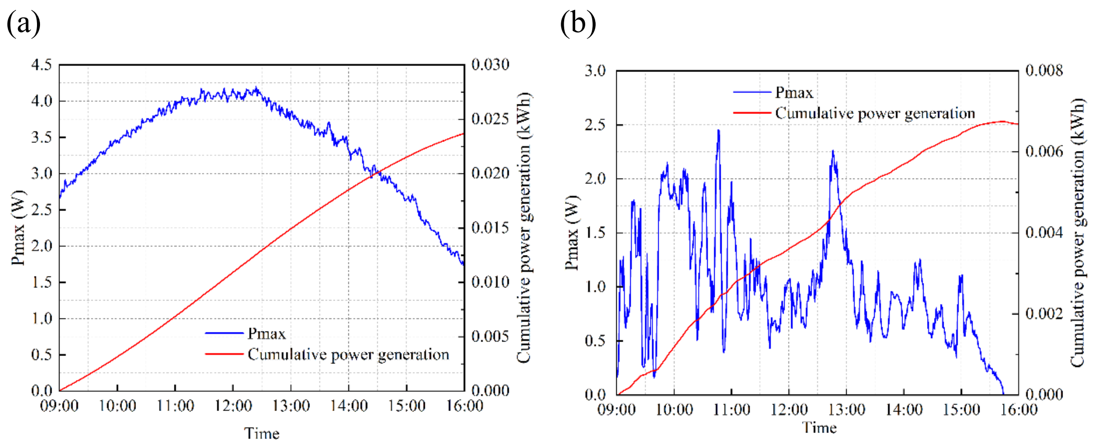

Fig. 5. The electricity generation of the system on (a) sunny days and (b) cloudy days

Fig. 6. shows the plots of the air inlet temperature, air outlet temperature and temperature difference between air inlet and air outlet, respectively. On sunny days, the air outlet temperature ranges from 23.7 to 35.6°C when the air inlet temperature ranges from 21.1 to23.9°C.. Similarly, on cloudy days, the air outlet temperature ranges from 22.7 to 26°C when the air inlet temperature ranges from 21.6 to 23.7°C. The temperature difference between air inlet and air outlet is 9.6°C and 3.9°C on sunny and cloudy days, respectively. On sunny days, the temperature difference between air inlet and air outlet of the T-wall system exceeds 10°C for approximately57% of the total experimental time. The air outlet temperature is posteriority compared to the solar

radiation intensity on sunny days. The air outlet temperature approached the maximum temperature at 13:40 p.m. Although the maximum temperature was obtained at 13:40 p.m., the air outlet temperature usually ascended until 14:29 p.m. Unlike sunny days, there is no clear pattern or regulation observed for the air outlet temperature on cloudy days. The air outlet temperature on cloudy days rises to 25.7°C at 10:27 a.m. and remains relatively stable at this value. It starts to decline after 13:32 p.m.

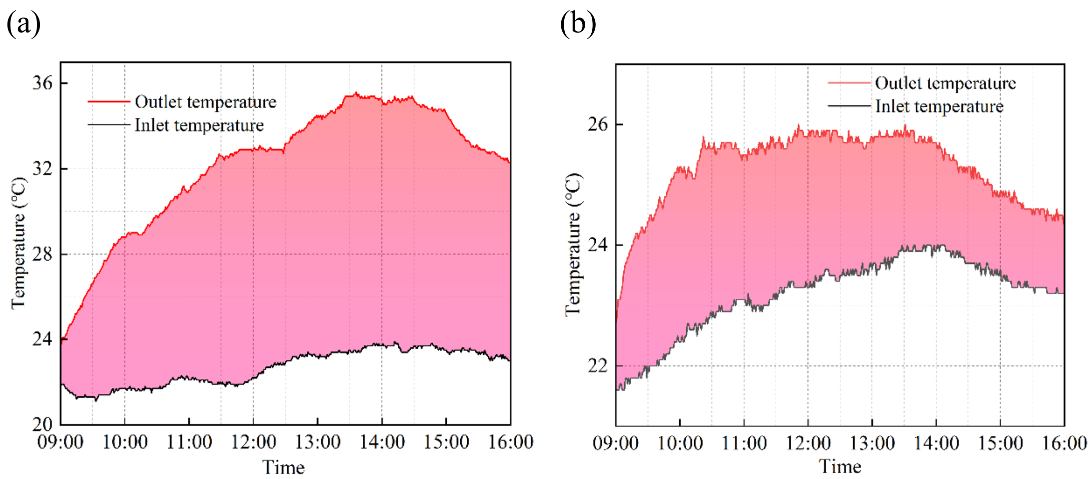

Fig. 6. The plots of the air inlet temperature, air outlet temperature on (a) sunny days and (b) cloudy days

Fig. 7. shows the solar heat gain of the T-wall system. According to the measurement results of the hot-wire anemometer, the airflow in the range of 0.01–0.096 m/s. The instantaneous heat gain can be calculated by the heat quantity formula, shown as **Eq. (9)**:

$$Q_{heat} = C_{Air} A V (T_{out} - T_{in}) \quad (9)$$

Where V, m/s is the airflow in the T-wall chamber and C_{Air}, J/(kg K) is the specific heat of air. T_{out} and T_{in} are air inlet temperature and air outlet temperature, respectively. A, m^2 is the area of the air outlet. The daily thermal efficiency, which is shown in **Eq. (10),** can be obtained from the time integral of **Eq. (9)**:

$$\overline{Q_{heat}} = \int C_{Air} A V (T_{out} - T_{in}) dt \quad (10)$$

The T-wall system can provide 17.74 kJ/mol heat on sunny days and 6.25 kJ/mol on cloudy days. The heat gain in the T-wall chamber is not solely determined by the solar radiation intensity. It is also influenced by the airflow within the T-wall chamber. The airflow plays a significant role in determining the heat gain, in addition to the temperature difference resulting from solar radiation intensity. From **Fig. 7,** it is evident that on sunny days, the heat gain remains consistently high from 11:49 a.m. to 14:36 a.m. Interestingly, the heat gain does not peak when the airflow reaches its maximum. This can be attributed to the fact that the temperature difference between the air inlet and air outlet is not at its maximum during that period (as shown in **Fig. 6**), resulting in a smaller heat gain. On cloudy days, The heat gain days reaches its maximum at 10:02 a.m. and subsequently decreases, following a similar trend as the airflow.

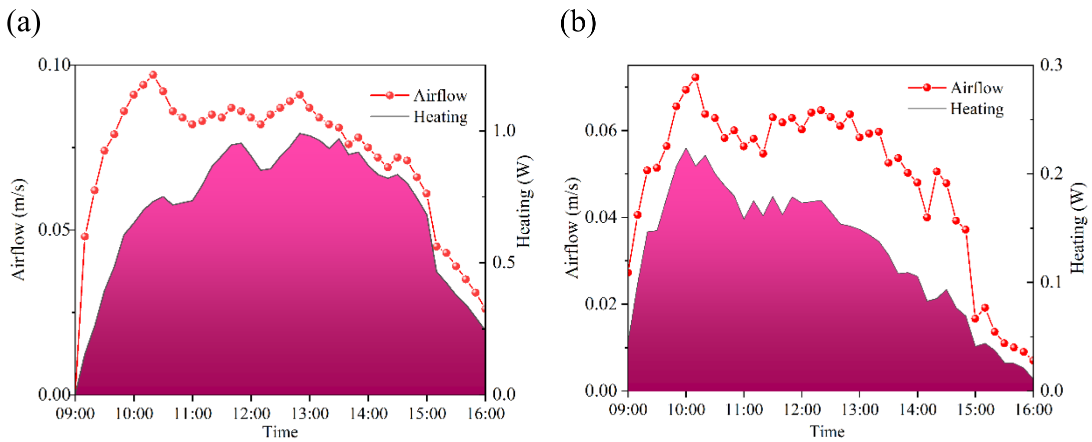

Fig. 7. The heat gain of the T-wall system on (a) sunny days and (b) cloudy days

To investigate the sterilization efficiency of the different bacterial aerosol concentrations, the sterilization efficiency of Serratia marcescens bioaerosols under experimental and control groups was measured. The control group has a similar structure to the experimental group, but it does not contain any catalytic material. The PV and aluminum panels in the experimental group were coated with photocatalytic membranes and thermal catalytic materials. The same dose of Serratia marcescens bacterial aerosol was sprayed at each hour to measure the change in sterilization efficiency over time. In this study, the concentration of sprayed bacterial aerosols was 1500±100 CFU/m^3. All sterilization efficiency in this study refers to one-way sterilization efficiency. The sterilization efficiency of bacterial aerosols is expressed as follows:

$$\eta_{sterilization}(\%) = (1 - \frac{CFU_{outlet}}{CFU_{inlet}}) \times 100\% \quad (11)$$

Where CFU_{outlet} and CFU_{inlet} are the concentration of bacterial aerosols at the outlet and inlet.

Fig. 8 shows the sterilization efficiency versus time of experimental and control groups. The sterilization efficiency of control group and experimental group were in the range of 0.172-0.208 and 0.204-0.347 calculated by **Eq.(11),** respectively. This shows that catalytic oxidization can effectively enhance the indoor air purification effect. The slow change in the sterilization efficiency curve over time for the control group indicates that the absence of catalytic oxidation in the control system limits its ability to effectively sterilize the air. In the control group, sterilization efficiency primarily relies on sedimentation. The sterilization efficiency of the experimental group was influenced by solar radiation. Sterilization efficiency reaches a maximum value of 0.347 at noon when solar radiation was at its peak. However, as solar radiation decreased throughout the day, the efficiency of sterilization gradually decreased as well. By the time of sunset, the sterilization efficiency of both the control and experimental groups had become equal.

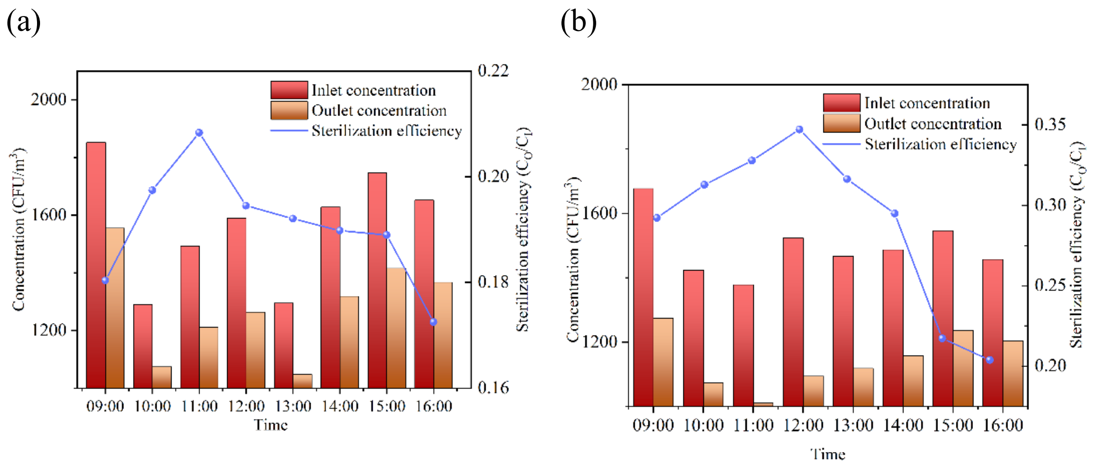

Fig. 8. The sterilization efficiency of (a) control group and (b) experimental group

The integration of catalytic oxidation and T-wall has led to a significant improvement in sterilization efficiency. The system achieved a one-way sterilization efficiency ranged from 0.204 to0.347 for bacterial aerosols, indicating promising application prospects for solar-powered indoor air purification. After long-term cyclic inactivation, the indoor bacterial aerosol concentration will descend to a harmless level.

4.2 Optimal spacing of the T-wall system

In this part, the performance of heating, electricity generation, and sterilization efficiency under different chamber spacing have been calculated. The chamber spacing is ranged from 35 cm to 15 cm, with an interval of 5 cm. The schematic diagram of the T-wall system spacing is shown in **Fig. 9**. It can be seen that the spacing has an important effect on the T-wall electricity generation performance. When the spacing is small, the baffles tend to block each other, resulting in reduced exposure to solar radiation.

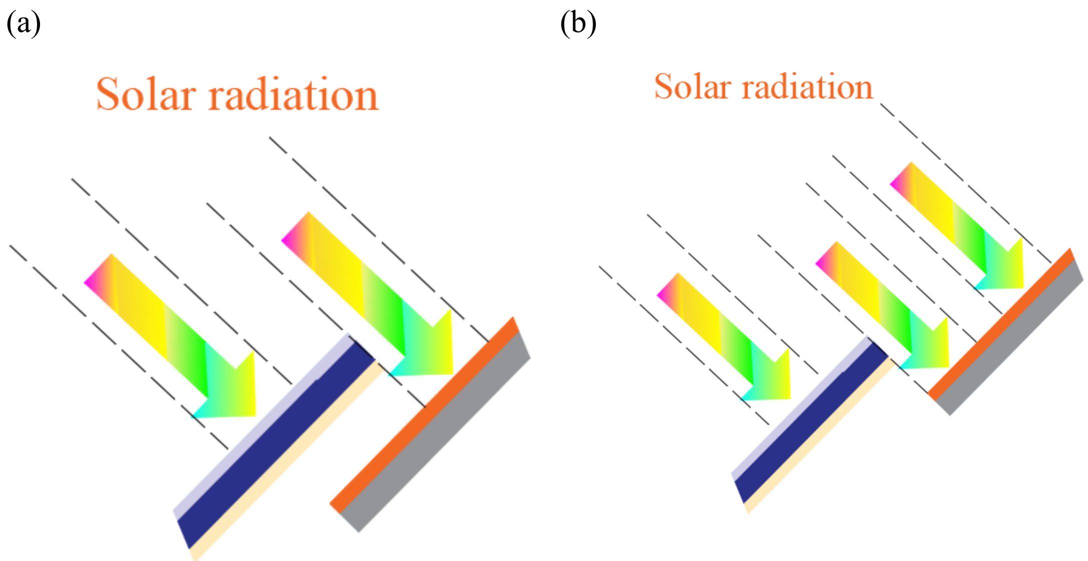

Fig. 9. Schematic diagram of T-wall system spacing. (a) small spacing and (b) large spacing

Fig. 10 shows the electricity generation of the T-wall system under different spacing. The electricity generation of the system continuously reduced as the spacing between the baffles decreased. The electricity generation of the system shows a similar trend across different spacing values. The average power observed for different spacing configurations, ranging from 35 cm, 30cm, 25cm, 20 cm to 15 cm, were 3.4 W, 3.0 W, 2.6 W, 2.1 W, and 1.4 W, respectively. This trend demonstrates that the spacing has an increasingly significant impact on the electricity generated as it decreases. Because when the spacing is reduced by 5 cm, the average electricity generation shows an increase from 0.4 W to 0.5 W, and finally reaches 0.7 W. When the spacing decreases from 35 cm to 15 cm, the cumulative electricity production per PV panel is 0. 0248 kWh, 0.0211 kWh, 0.0188 kWh, 0.0146 kWh, and 0.0101 kWh, respectively. Similar to the average power, the cumulative electricity generation does not reduce equally as the spacing decreases. An inflection point occurs at 25cm, where the reduction in system electricity generation increases for every 5cm reduction in spacing.

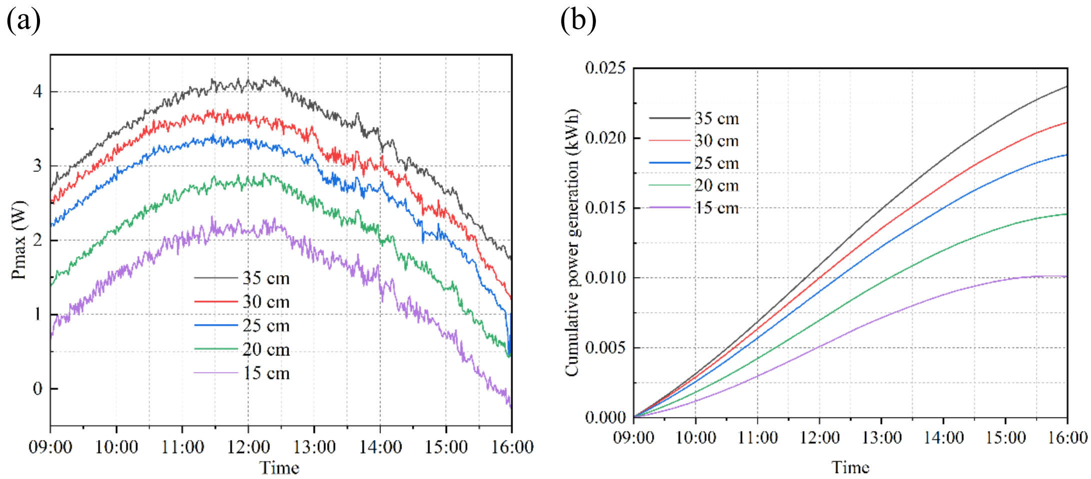

Fig. 10. The electricity generation of the T-wall system under different spacing. (a) power and (b) cumulative power generation

For bacterial aerosol concentration, it is mainly affected by sedimentation and catalytic oxidation. The impact of sedimentation has been analyzed in the control group in **Section 4.1.** The reaction rate of photocatalysis is shown in **Eq. (12)**:

$$r = -\frac{dC_s}{dt} = \frac{k_r K C_s}{(1+KC_s)} \tag{12}$$

Where r, mg/(L*min), is the reaction rate. C_s, mg/L, is the pollutant concentration. t, min, is the reaction time. k_r, min^{-1}, is the reaction rate constant. K is the adsorption constant. k_r and K is determined by many factors in the reaction, including light intensity, initial concentration of pollutants, reaction temperature, physical properties of reactants, oxygen concentration, etc.

Fig. 11 shows the sterilization efficiency of the T-wall system under different spacing. The sterilization efficiency increased as the spacing decreased . Similar to the **Section 4.1**, sterilization efficiency reaches its maximum value at noon. The average sterilization efficiency for spacing values of 35 cm, 30 cm, 25 cm, 20 cm, and 15 cm are 0.365, 0.356, 0.343, 0.267, and 0.202, respectively. The highest sterilization efficiency of 0.448 can reached when the spacing is 15cm. When the spacing is decreased to 25cm, further decreasing the spacing has minimal impact on improving bacterial sterilization efficiency. This can be explained as the adsorption of bacterial aerosols on catalyst surfaces. As can be seen from **Eq. (12),** reaction time has an effect on catalytic sterilization. The reaction rate of the bacterial aerosol decreases as the reaction time with the catalyst increases. As the spacing decreases, the volumetric flow rate of the bacterial aerosol increases, which can affect the catalytic oxidation reaction. The volumetric flow rate effect is ultimately manifested by the adsorption of pollutant gas molecules on the catalyst surface. Once the spacing is decreased to 25cm, the volumetric flow rate has approached its maximum value. Further reduction of the spacing has limited effect on the volumetric flow rate, resulting in minimal increase in the reaction rate. From an efficiency perspective, the spacing of 25 cm can be the optimal sterilization efficiency spacing for the T-wall system.

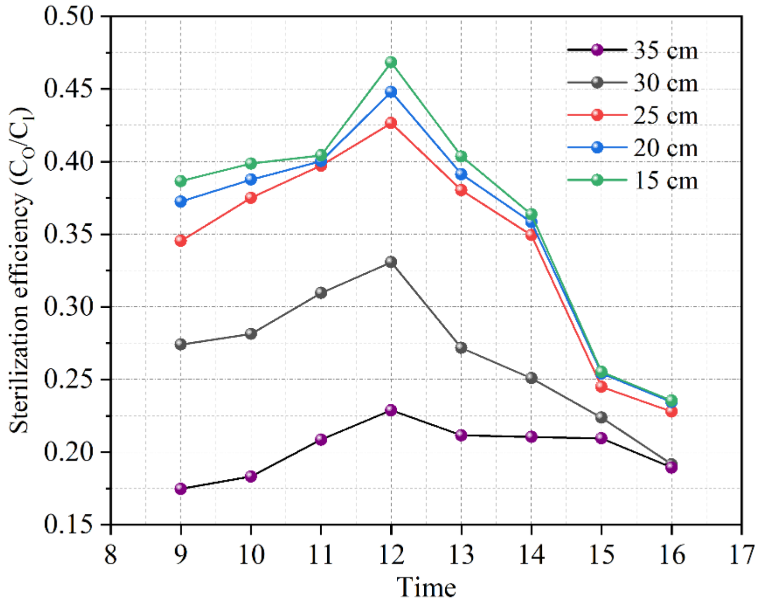

Fig. 11. The sterilization efficiency of the T-wall system under different spacing

Thermal efficiency was used to evaluate the system's ability in converting solar radiation into heat. The thermal efficiency of the system is evaluated by the proportion of thermal energy obtained from the air in the T-wall chamber to the total received solar radiation of the system. The expression is as **Eq. (13)**:

$$\eta_T = \frac{C_{air} V A_{out} (T_{out} - T_{in})}{A_{solar} I_{solar}} \quad (13)$$

Where T_{out} and T_{in} are the air outlet and inlet temperature. A_{out}, m^2, is the area of the air outlet. A_{solar}, m^2, is the received area of solar radiation. I_{solar}, W/ m^2, is the solar radiation intensity.

Fig. 12 shows the thermal efficiency of the T-wall system under different spacing. The thermal efficiency was increased with time. Due to the hysteresis of heat transfer, The curve between thermal efficiency and solar radiation is not similar. Even when solar radiation decreases, the T-wall system continues to heat the air, leading to a sustained thermal efficiency. When the spacing is reduced from 35cm to 15cm, the thermal efficiency of the T-wall system increases. The thermal efficiency values observed are 0.05, 0.075, 0.098, 0.103, and 0.121, respectively. This trend is similar to the trend observed for sterilization efficiency, indicating that reducing the spacing will improve thermal efficiency. When the spacing is reduced to 25cm, further reducing has a limited effect on improving the thermal efficiency.

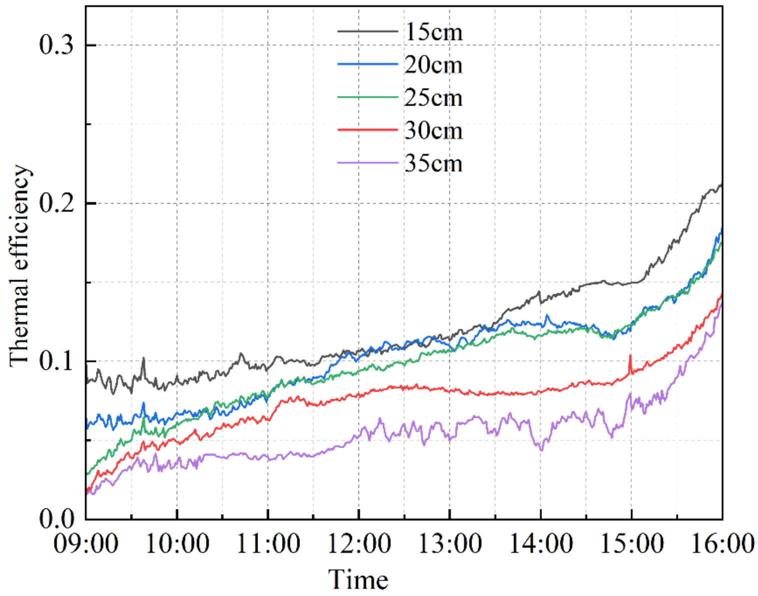

Fig. 12. The thermal efficiency of the T-wall system under different spacing

Due to the obstruction of the baffle, solar radiation cannot directly heat the air inside the system cavity. The temperature rise of the air in the T-wall system chamber is mainly achieved through convective and radiative heat transfer through baffles. Reducing the spacing increases the volume flow rate, which enhances convective heat transfer with the baffle. Additionally, according to **Eq. (13)**, increasing the flow rate improves thermal efficiency. Limited by volume flow rate, the optimal spacing for thermal efficiency spacing in the T-wall system is found to be 25 cm, similar to the optimal spacing for sterilization efficiency.

Based on the analysis of heating, electricity generation, and sterilization efficiency, the optimal spacing for the T-wall system is determined to be 25 cm. This spacing allows for effective sterilization, efficient heating, and maximum electricity generation.

4.3 Optimization of layout of UV light strips for sterilization efficiency

UV radiation a widely employed method for control bioaerosol due to its germicidal effect. UV radiation also serves as the driving force for photocatalytic oxidation, making it an effective method for indoor sterilization and disinfection. In this study, we have arranged UV light strips inside the T-wall system chamber as shown in **Fig. 13**. The total length of the light strip is 0.6 m, which is the same as the T-wall system. The UV light strips used in this study are consisted of one light bead every 10cm. Each light bead can give 600 $\mu W/cm^2$ radiation intensity. The lights emitted short-wave UV radiation with a radiation peak at 253.7 nm for germicidal action. The ultraviolet light strip in the T-wall system is powered by the PV panels, with three PV panels being used to provide the necessary energy.

Fig. 13. The photograph of UV light strips

The system is equipped with a total of four UV light strips. The layout of UV light would have an impact on sterilization efficiency by affecting the UV dose. UV dose was calculated with the following equations:

$$UV\ dose\ (mJ/cm^2) = radiation\ intensity\ (\mu W/cm^2) \times radiation\ time\ (s)$$

Specific UV dose depends on the residence time of the bacterial bioaerosols in the zone. **Fig. 14** shows the different layouts of UV light strips. In this study, three layouts were used: (a) balanced arrangement (b) inlet and outlet arrangement (c) up and down arrangement. The balanced arrangement is designed to arrange the UV light strips at the same spacing on the surface of the thick walls. The inlet and outlet arrangement is designed to concentrate two UV light strips at the air inlet and two UV light strips at the air outlet.. Up and down arrangement is designed to install two UV light strips at the top and two UV light strips at the bottom of the T-wall system.

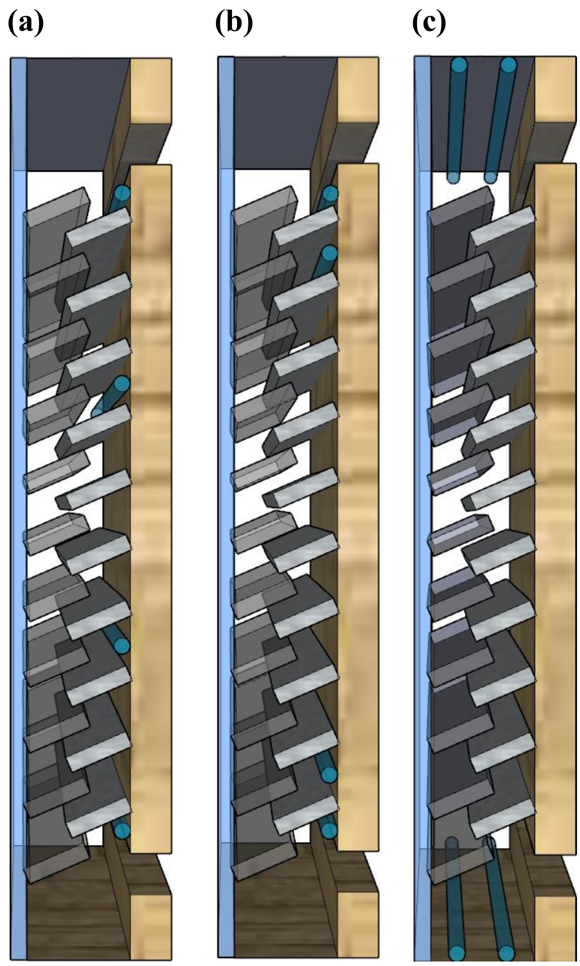

Fig. 14. The different layouts of UV light strips. (a) balanced arrangement (b) inlet and outlet arrangement (c) up and down arrangement.

As shown in **Fig.15**, the installation of UV light strips significantly improved the sterilization efficiency, approaching levels of approximately 20–50% regardless of the layout. Similar to the solar radiation intensity, the sterilization efficiency of the system curve also presents the parabola-type trend. The sterilization efficiency increases with the increasing of solar radiation. This can be attributed to two factors. Firstly, solar radiation affects the sterilization of bacterial aerosols through photocatalytic and thermal catalytic oxidation. Secondly, solar radiation also powers the UV light strips, increasing their radiation intensity as solar radiation intensity rises. Then sterilization efficiency reaches its peak at noon when solar radiation intensity is highest. Subsequently, as the decrease in solar radiation intensity, the sterilization efficiency gradually decreases.

As to the layout of UV light strips, it can be seen from **Fig.15**, the top and bottom arrangement has better sterilization efficiency. Sterilization efficiency was in the range of 0.24-0.49 for the whole day and approached 0.49 at noon. The installation of UV light strips at the top and bottom of the system effectively inactivates many bacterial aerosols through irradiation. In addition, the UV light strips located at the top of the system emit radiation onto the photocatalytic membrane, enabling photocatalytic oxidation to take place. Both the radiation intensity of the UV light strips and the catalytic oxidation are significantly influenced by solar radiation. When solar radiation is reduced, a significant decrease in sterilization efficiency can be observed. However, the top and bottom arrangement experiences a faster decrease in sterilization efficiency compared to the other two arrangements as solar radiation decreases. This may due to the open space at the top and bottom of the T-wall system, bacterial aerosols carried by the airflow have a tendency to accumulate in these areas. As for the balanced arrangement and inlet and outlet arrangement of UV light strips, they are designed to irradiate the airflow path, which significantly improve the sterilization efficiency when compared to the syetem without UV light strips. The sterilization efficiency of the balanced arrangement and inlet and outlet arrangement presents a similar variation trend with the top and bottom arrangement. The sterilization efficiency of the balanced arrangement and inlet and outlet arrangement were in the range of 0.249-0.408 and 0.234-0.377, respectively. Due to the presence of the baffle, the radiation area for UV light strips in both the balanced arrangement and inlet and outlet arrangement is limited, and the air flow has less exposure time to the radiation. As a result, sterilization efficiency of these arrangement is lower compared to the top and bottom arrangement.

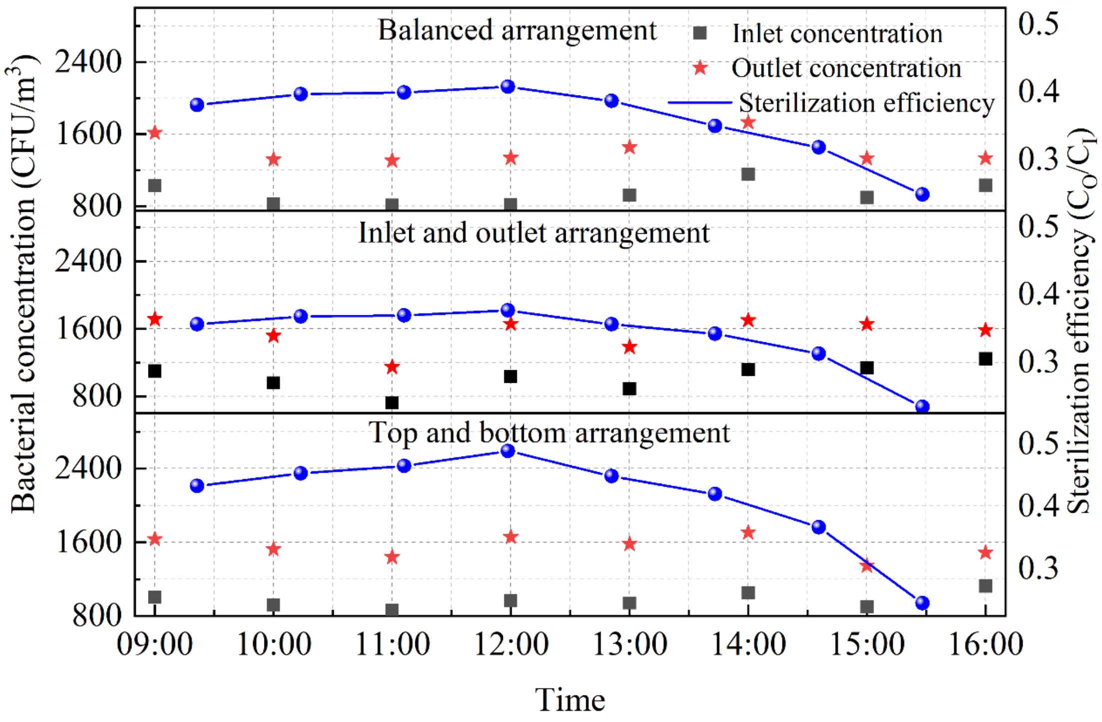

Fig. 15. The sterilization efficiency of different layouts of UV light strips

5. Conclusion

A novel Trombe wall was proposed to simultaneously address heating, electricity, and indoor air quality improvement. The performance of heating and electricity generation performance, optimal spacing of the T-wall system, and the impact of different concentrations and layout of UV light strips on sterilization efficiency of were investigated. The main conclusions are summarized as follows:

(1) The optimized T-wall system demonstrated a power generation range of 0.06 kWh to 0.298 kWh power and heat output ranging from 6.25 kJ/mol to 17.74 kJ/mol, making it suitable for winter conditions in severe cold regions. The system achieves a sterilization efficiency of 0.204-0.347, making it highly promising for solar-powered indoor air purification applications.

(2) The spacing between the baffles in the T-wall system has a significant impact on airflow, heating, electricity generation, and sterilization efficiency. The optimal spacing for the system is found to be 25 cm, as it meets the sterilization efficiency

and heating and balances electricity generation.

(3) The sterilization efficiency of the system was further enhanced by the arrangement of UV light strips in the T-wall system. The layout of the top and bottom arrangement facilitates catalytic reactions, resulting in higher sterilization efficiency.

Authors' contributions

Xiaojian Duan: Writing, Investigation, Data analysis.

Chao Shen: Supervision, Writing, Investigation, Resources.

Yuoeng Wu: Supervision.

Declaration of conflicting interests

The author(s) declare no potential conflicts of interest with respect to the research, authorship, and/or publication of this article.

Acknowledgement

The author(s) disclosed receipt of the following financial support for the research, authorship, and/or publication of this article: The authors gratefully acknowledge the funding supports from the National Natural Science Foundation of China (Project#: 52178071).

Reference

1. Li JH, Zhang W, Xie LZ, et al. A hybrid photovoltaic and water/air based thermal(PVT) solar energy collector with integrated PCM for building application. *Renew Energ.* 2022;199:662-671.

2. Agathokleous RA, Kalogirou SA, Karellas S. Exergy analysis of a naturally ventilated Building Integrated Photovoltaic/Thermal (BIPV/T) system. *Renew Energ.* 2018;128:541-552.

3. Savvides A, Vassiliades C, Michael A, Kalogirou S. Siting and building-massing considerations for the urban integration of active solar energy systems. *Renew Energ.* 2019;135:963-974.
4. Bordbari MJ, Seifi AR, Rastegar M. Probabilistic energy consumption analysis in buildings using point estimate method. *Energy.* 2018;142:716-722.
5. Li N, Gu T, Xie H, Ji J, Liu X, Yu B. The kinetic and preliminary performance study on a novel solar photo-thermal catalytic hybrid Trombe-wall. *Energy.* 2023;269:126839.
6. Du L, Ping L, Chen YM. Study and analysis of air flow characteristics in Trombe wall. *Renew Energ.* 2020;162:234-241.
7. Yu BD, Fan MM, Gu T, Xia XK, Li NS. The performance analysis of the photo-thermal driven synergetic catalytic PV-Trombe wall. *Renew Energ.* 2022;192:264-278.
8. Jiang B, Ji J, Yi H. The influence of PV coverage ratio on thermal and electrical performance of photovoltaic-Trombe wall. *Renew Energ.* 2008;33(11):2491-2498.
9. Wu SY, Xu L, Xiao L. Air purification and thermal performance of photocatalytic-Trombe wall based on multiple physical fields coupling. *Renew Energ.* 2020;148:338-348.
10. Ma QS, Fukuda H, Wei XD, Hariyadi A. Optimizing energy performance of a ventilated composite Trombe wall in an office building. *Renew Energ.* 2019;134:1285-1294.
11. Abed AA, Ahmed OK, Weis MM, Hamada KI. Performance augmentation of a PV/Trombe wall using Al2O3/Water nano-fluid: An experimental investigation. *Renew Energ.* 2020;157:515-529.
12. Koyunbaba BK, Yilmaz Z. The comparison of Trombe wall systems with single glass, double glass and PV panels. *Renew Energ.* 2012;45:111-118.
13. Jie J, Hua Y, Gang P, Bin J, Wei H. Study of PV-Trombe wall assisted with DC fan. *Build Environ.* 2007;42(10):3529-3539.
14. Kong XF, Li JB, Fan M, Li W, Li H. Study on the thermal performance of a new double layer PCM trombe wall with multiple phase change points. *Sol Energ Mat Sol C.* 2022;240.
15. Zhang ZG, Liu QL, Yao WX, Zhang W, Cao JF, He HY. Research on temperature distribution characteristics and energy saving potential of wall implanted with heat pipes in heating season. *Renew Energ.* 2022;195:1037-1049.
16. Liu ZB, Zhang L, Gong GC, Han TH. Experimental evaluation of an active solar thermoelectric radiant wall system. *Energ Convers Manage.* 2015;94:253-260.
17. Luo YQ, Zhang L, Liu ZB, Wang YZ, Wu J, Wang XL. Dynamic heat transfer modeling and parametric study of thermoelectric radiant cooling and heating panel system. *Energ Convers Manage.* 2016;124:504-516.
18. Luo YQ, Zhang L, Liu ZB, Wu J, Zhang YL, Wu ZH. Numerical evaluation on energy saving potential of a solar photovoltaic thermoelectric radiant wall system in cooling dominant climates. *Energy.* 2018;142:384-399.
19. Zhu N, Li SS, Hu PF, Lei F, Deng RJ. Numerical investigations on performance of phase change material Trombe wall in building. *Energy.* 2019;187.
20. Duan SP, Wang L, Zhao ZQ, Zhang CW. Experimental study on thermal performance of an integrated PCM Trombe wall. *Renew Energ.* 2021;163:1932-1941.
21. W. He, C.C. Wang, J. Ji. Study on the effect of trombe wall with Venetian blind structure on indoor temperature in different blade angle. Taiyangneng Xuebao/Acta Energiae Solaris Sinica, 37 (2016), pp. 673-67.

22. Agarwal N, Meena CS, Raj BP, et al. Indoor air quality improvement in COVID-19 pandemic: Review. *Sustain Cities Soc.* 2021;70.
23. Duan XJ, Shen C, Chen DQ, Zhai ZQ. Effect of environmental factors on the concentration distribution of bioaerosols with different particle sizes in an enclosed space. *Indoor Built Environ.* 2023;32(2):408-424.
24. Yu BD, Yang JC, He W, Qin MH, Zhao XD, Chen HB. The performance analysis of a novel hybrid solar gradient utilization photocatalytic-thermal-catalytic-Trombe wall system. *Energy.* 2019;174:420-435.
25. Yang X, Wang Y. Photocatalytic effect on plasmid DNA damage under different UV irradiation time. *Building and Environment.* 2008;43(3):253-257.
26. Morawska L, Tang JLW, Bahnfleth W, et al. How can airborne transmission of COVID-19 indoors be minimised? *Environ Int.* 2020;142.
27. Banik RK, Ulrich A. Evidence of Short-Range Aerosol Transmission of SARS-CoV-2 and Call for Universal Airborne Precautions for Anesthesiologists During the COVID-19 Pandemic. *Anesth Analg.* 2020;131(2):E102-E104.
28. GB/T. 50189-2015. Design standard for energy efficiency of public buildings (2015). (in Chinese).
29. JGJ. 26-2010. Design standard for energy efficiency of residential buildings in severe cold and cold regions (2010). (in Chinese).
30. Cowling BJ, Ip DKM, Fang VJ, et al. Aerosol transmission is an important mode of influenza A virus spread. *Nat Commun.* 2013;4.
31. Guo KQ, Qian H, Zhao DL, et al. Indoor exposure levels of bacteria and fungi in residences, schools, and offices in China: A systematic review. *Indoor Air.* 2020;30(6):1147-1165.
32. Wang ZJ, Xue QW, Ji YC, Yu ZY. Indoor environment quality in a low-energy residential building in winter in Harbin. *Build Environ.* 2018;135:194-201.
33. Zhang RM, Song CJ, Kou MP, et al. Sterilization of Escherichia coli by Photothermal Synergy of WO3-x/C Nanosheet under Infrared Light Irradiation. *Environ Sci Technol.* 2020;54(6):3691-3701.
34. Liao JJ, Xu YD, Zhao YY, Wang CC, Ge CJ. Ag and Fe3O4 Comodified WO3-x Nanocomposites for Catalytic Photothermal Degradation of Pharmaceuticals and Personal Care Products. *Acs Appl Nano Mater.* 2021;4(2):1898-1905.
35. Zhang J, Li JS, Zhang QX, Guo DG. Constructing a novel CuS/Cu2S Z-scheme heterojunction for highly-efficiency NIR light-driven antibacterial activity. *Appl Surf Sci.* 2023;624.
36. Zhang Z, Sun JY, Chen X, et al. Unraveling the role of defect types in Fe3O4 for efficient NIR-driven photocatalytic inactivation. *Appl Surf Sci.* 2023;622.
37. Yu BD, He W, Li NaS, Yang F, Ji J. Thermal catalytic oxidation performance study of SWTCO system for the degradation of indoor formaldehyde: Kinetics and feasibility analysis. *Build Environ.* 2016;108:183-193.
38. Vivar M, Skryabin I, Everett V, Blakers A. A concept for a hybrid solar water purification and photovoltaic system. *Sol Energ Mat Sol C.* 2010;94(10):1772-1782.
39. Yu BD, Li NS, Yan CC, et al. The comprehensive performance analysis on a novel high-performance air-purification-sterilization type PV-Trombe wall. *Renew Energ.* 2022;182:1201-1218.
40. Yu BD, He W, Li NS, et al. Experiments and kinetics of solar PCO for indoor air purification in PCO/TW system. *Build Environ.* 2017;115:130-146.

41. Bai BY, Qiao Q, Li JH, Hao JM. Progress in research on catalysts for catalytic oxidation of formaldehyde. *Chinese J Catal.* 2016;37(1):102-122.
42. Zhang TT, Tan YF, Yang HX, Zhang XD. The application of air layers in building envelopes: A review. *Appl Energ.* 2016;165:707-734.
43. Mcguigan KG, Joyce TM, Conroy RM, Gillespie JB, Elmore-Meegan M. Solar disinfection of drinking water contained in transparent plastic bottles: characterizing the bacterial inactivation process. *J Appl Microbiol.* 1998;84(6):1138-1148.
44. Yu BD, Li NaS, Xie H, Ji J. The performance analysis on a novel purification-cleaning trombe wall based on solar thermal sterilization and thermal catalytic principles. *Energy.* 2021;225.
45. Yu BD, Li NS, Ji J. Performance analysis of a purified Trombe wall with ventilation blinds based on photo-thermal driven purification. *Appl Energ.* 2019;255.
46. Yu BD, Liu XY, Li NS, Liu SS, Ji J. The performance analysis of a purified PV/T-Trombe wall based on thermal catalytic oxidation process in winter. *Energ Convers Manage.* 2020;203.
47. Zhang CX, Shen C, Zhang YB, Sun C, Chwieduk D, Kalogirou SA. Optimization of the electricity/heat production of a PV/T system based on spectral splitting with Ag nanofluid. *Renew Energ.* 2021;180:30-39.
48. Xiao KM, Wang TQ, Sun MZ, et al. Photocatalytic Bacterial Inactivation by a Rape Pollen-MoS2 Biohybrid Catalyst: Synergetic Effects and Inactivation Mechanisms. *Environ Sci Technol.* 2020;54(1):537-549.